Hindawi
Journal of Nanomaterials
Volume 2019, Article ID 3059098, 9 pages
https://doi.org/10.1155/2019/3059098

Research Article

Ultrafine Nanoparticles of Poly(Methyl Methacrylate-*co*-Methacrylic Acid) Loaded with Aspirin

R. López-Muñoz, M. E. Treviño, G. Morales, J. A. Valdez-Garza, R. Díaz de León, H. Saade, F. J. Enríquez-Medrano, and R. G. López

Centro de Investigación en Química Aplicada, Blvd. Enrique Reyna, 140, 25294 Saltillo, Mexico

Correspondence should be addressed to R. G. López; guillermo.lopez@ciqa.edu.mx

Received 30 April 2019; Revised 9 July 2019; Accepted 22 July 2019; Published 14 August 2019

Academic Editor: Loretta L. Del Mercato

Nanoparticles of the poly(methyl methacrylate-*co*-methacrylic acid) or copolymer of P(MMA-*co*-MAA), were prepared by semicontinuous heterophase polymerization; they show a mean diameter of 12 nm and a 1.75 MMA/MAA molar ratio determined by carbon-13 nuclear magnetic resonance. The content of MAA, greater than that of Eudragit S100, copolymer of P(MMA-*co*-MAA) accepted by the FDA for the preparation of tablets, ensures its biocompatibility and its metabolism without toxic effects. Loaded with up to 22 wt. % aspirin, that is, acetylsalicylic acid (ASA), these nanoparticles increase slightly their size, according to transmission electron microscopy; however, the presence of ASA on the nanoparticle surface decreases their stability, which leads to a certain aggregation of the particles in the dispersion. Fourier transform infrared spectrometry was used for demonstrating the loading of ASA in the nanoparticles.

1. Introduction

Biodegradable and biocompatible ultrafine nanoparticles are considered as ideal vehicles for drug delivery. The main expected advantages of this type of nanosystems with respect to the use of the free drug are claimed to be an increased efficiency, longer circulation time in the bloodstream, protection against degradation, and specifically in antineoplastic therapy, attenuation of side effects and overcoming of multidrug resistance [1–4]. Recently, an increased attention has been devoted to the research of polymeric nanoparticles as vehicle for immunotherapy [5] and photothermal therapy [6].

The research on drug-loaded nanostructures began some decades ago; however, the products resulting from this great task are relatively few. For example, in the case of antineoplastic-loaded nanostructures, at present, there are only less than 20 products in clinical use [7–10]. Among the main reasons behind the low number of drug-loaded nanostructures with FDA approval are those related to their characteristic size as well as the biocompatibility and biodegradability of the material that forms the nanostructures. It has been proven that nanostructures with sizes less than 8-10 nm are not appropriate because the kidneys would filter them [11]. Likewise, sizes greater than 100 nm are not desirable either because the immunological system, as well as the liver and the spleen, withdraw nanostructures with these sizes from the bloodstream [1, 12]. Then, taking into account only the sizes, the nanostructures ranging from 10 to 100 nm in size would have the highest chances to remain in the bloodstream either to slowly release the drug or to reach the tumors, in the case of antineoplastic therapies. Therefore, considering that the smaller the size, the greater the probability of the nanostructures to evade the immunological system [13], sizes slightly greater than 10 nm are advisable for drug-loaded nanostructures.

Recently, a method to prepare ultrafine nanoparticles with mean diameter close to 10 nm by *semicontinuous heterophase polymerization* (SCHP) was reported by our group [14]. The material of these nanoparticles is a poly(methyl methacrylate-*co*-methacrylic acid) copolymer (CNP, or poly(MMA-*co*-MAA)), which is biocompatible and could be removed from the organism without toxic residues

because it turns water soluble at pH > 7. In fact, this copolymer is similar in composition to that of Eudragit S100® (ES-100), material approved by the FDA and widely used as excipient in the manufacture of drug tablets used to treat various diseases [15]. The preparation of ibuprofen-loaded nanoparticles of this copolymer with diameters close to 10 nm has been reported by our group [16].

In order to use the CNP as a vehicle for the administration of drugs, the loading of ASA in CNP was first investigated. A review of the literature indicates that despite intensive research on the loading of ASA in micro- and nanostructures [17–25], there are no reports on the preparation of solid nanoparticles of FDA-approved polymers, with diameters close to 10-20 nm, loaded with this drug. Due to their small size, these nanosystems would have a high probability of circulating for long periods of time in the bloodstream, slowly releasing the drug, reducing the dosage frequency.

Herein, we document the obtaining of CNP using the method reported by our group [14], including the molecular weight determination in the characterization of the copolymer, which was not considered in that previous report. Likewise, the ASA loading of the nanoparticles and the characterization of the resulting system is reported.

2. Materials and Methods

2.1. Materials. Sodium dodecyl sulfate (SDS) (98.5%), sodium bis(2-ethylhexyl) sulfosuccinate (AOT) (96%), ammonium persulfate (APS) (99%), and acetylsalicylic acid (ASA) (≥99%) from Sigma-Aldrich were used as received. MMA and MAA also from Sigma-Aldrich were distilled under reduced pressure and stored at 4°C. Dichloromethane (DCM) (>99%) from CTR Scientific was used as received. Deionized and triple-distilled (ultrapure) water with conductivity less than 6 μS/cm was used. Tetrahydrofuran (THF, HPLC grade), (trimethylsilyl)diazomethane solution in hexanes, deuterated chloroform, and deuterated trifluoroacetic acid from Sigma-Aldrich were used as received.

2.2. Methods

2.2.1. Polymerization. A solution containing 93 g of water, 0.1 g of APS, and 1.25 g of a mixture of surfactants SDS/AOT, 3/1 (wt/wt), was prepared in a 150 mL glass jacketed reactor. Then, the solution, under mechanical stirring at 650 rpm, was bubbled with argon for 1 h and heated up to 70°C, after which 12.6 g of MMA/MAA, 2/1 (mol/mol), was dosed at constant flow for one hour. At the end of the monomer addition, the reaction was allowed to proceed for an additional 30 min; samples were taken from the final dispersion to carry out the characterization.

2.2.2. Loading. The latex obtained through SCHP was dialyzed to remove the surfactants and then diluted with ultrapure water to 1% of solids content, adjusting the pH to 5, using 0.1 N NaOH solution. In a glass vial, 10 g of the purified latex was put in contact with 30 g of a solution of ASA in DCM at 0.1, 0.2, 0.4, or 0.6 wt. %, at 35°C during 12 hours. According to the boiling point of DCM, as well as DCM and water densities, the loading was completed when the whole DCM was evaporated. The resulting latex was filtered and characterized. All loading experiments were carried out by duplicate.

To determine the ASA content in the loaded nanoparticles, the procedure was as follows. At the end of the test, a sample of the latex containing the loaded nanoparticles was taken to determine solids content, and from this value, the total solids in the latex of the loaded nanoparticles (W_T) was calculated. Additionally, another sample of the latex was taken to be subjected to ultracentrifugation in an Optima XL-100 K ultracentrifuge at 50,000 rpm for 3 hours. At the end of this operation, a sample of the supernatant was taken to measure solids content, which was determined by the ASA remaining dissolved in the aqueous phase, that is, the drug not loaded in the nanoparticles. From this value, the amount of ASA that was not incorporated to the nanoparticles (W_{RA}) was calculated. In order to know the real weight of the loaded nanoparticles (W_L), W_{RA} was subtracted to W_T. The content of ASA in the loaded nanoparticles was calculated by the following equation:

$$\text{ASA loaded}\,(\%) = \frac{(W_L - W_N)}{W_L} * 100, \quad (1)$$

where W_N is the amount of CNP used in the test.

The loading efficiency, on the other hand, was calculated using

$$\text{Loading efficiency}\,(\%) = \frac{(W_L - W_N)}{W_{IA}} * 100, \quad (2)$$

where W_{IA} is the amount of ASA used in the corresponding loading test.

2.3. Characterization

2.3.1. Quasielastic Light Scattering (QLS). Measurements by QLS were carried out in a Malvern Zetasizer Nano-ZS90 apparatus at 25°C to determine the number-average diameter (D_n) of the latexes before and after the dialysis step and after the loading process. To eliminate multiple scattering and particle interactions, the latex samples were diluted 50 times with water.

2.3.2. Transmission Electron Microscopy (TEM). The nanoparticle diameters were also determined by TEM in a high-resolution transmission electron microscope FEI TECNAI G2 F30; the samples were prepared by dispersing both the latex before and after the loading process in 50 g of deionized water containing 0.01% of mannitol as coating material. Then, a drop of the resulting dispersion was deposited on a copper grid and analyzed after the water evaporation.

2.3.3. Gel Permeation Chromatography (GPC). A sample of the dialyzed latex was subjected to three freezing-and-thaw cycles for the copolymer coagulation, then was filtered, washed with deionized water, and dried. After this, both the copolymer prepared and a sample of ES-100 were dissolved in a mixture of tetrahydrofuran/methanol (70/30 *v*/*v*) adding afterwards a few drops of (trimethylsilyl) diazomethane

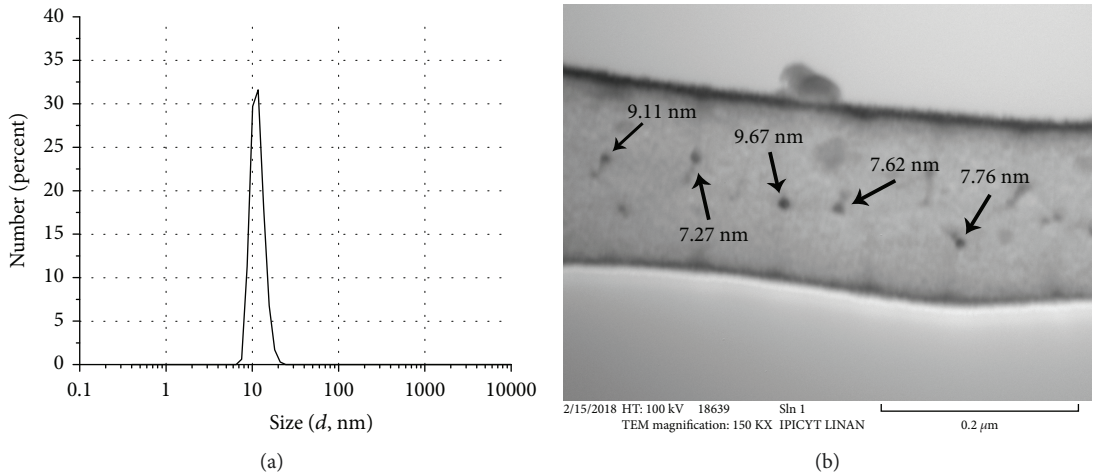

(a) (b)

Figure 1: (a) Particle size distribution obtained by QLS of a latex sample from copolymerization of MMA/MAA (2/1, mol/mol); (b) TEM micrograph from the same sample.

solution in hexane to methylate the MAA units of the copolymer. The dried methylated copolymer was dissolved in THF and analyzed in a Hewlett-Packard instrument (HPLC series 1100) equipped with a refractive index detectors. A PLGel mixed column was used. Calibration was carried out with poly(methyl methacrylate) standards from Sigma-Aldrich ranging from 2,000 to 2.48×10^6 g/mol, using THF HPLC grade as eluent at a flow rate of 1 mL/min.

2.3.4. Fourier Transform Infrared Spectrometry (FTIR). This technique was used to analyze the ES-100, as well as the loaded and unloaded copolymer nanoparticles in a Nicolet Magna-IR 550 spectrometer in ATR mode, with 25 scans at room temperature.

2.3.5. Nuclear Magnetic Resonance (NMR). The unloaded CNP and the ES-100, as reference, were analyzed by ^{13}C-NMR (12,000 scans) in a Bruker-400 MHz spectrometer. A mixture of deuterated chloroform and deuterated trifluoroacetic acid (50/50 *v*/*v*) was used as solvent, and the analysis was performed at room temperature.

2.3.6. Zeta Potential Measurements. These analyses were carried out in a Zetasizer Nano ZS equipment from Malvern Instruments Ltd., UK. The pH of the latex was adjusted to the required values using HCl or NaOH aqueous solutions, both at 0.1 N.

3. Results and Discussion

3.1. Polymeric Nanoparticles

3.1.1. Particle Size. As a result of the polymerization, nanoparticles were obtained in an aqueous dispersion in which they represented 12 wt. %. Figure 1 shows the particle size distribution obtained by QLS, as well as a micrograph from a sample of the dispersion. The number-average diameter (D_n) determined by QLS is 12 nm, which matches very well with that shown in the micrograph. These results are similar to those obtained in our previous reports [14, 16]. The total absence in the specialized literature of reports, with the exception of ours, on the preparation of poly(MMA-*co*-MAA), 2/1 (mol/mol) or close to this molar ratio (as will be demonstrated later) in nanoparticles as small as those here obtained, is worth noting.

These sizes are possible due to polymerization by SCHP operating under monomer-starved conditions. As previously explained [14], these conditions favor the particle nucleation instead the growth of those already formed, which leads to obtain very tiny particles.

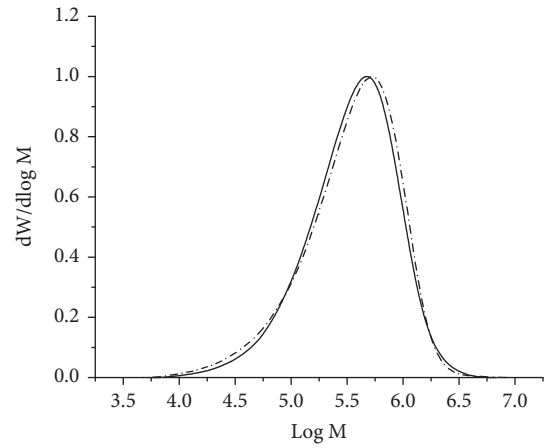

Figure 2: Molecular weight distribution of a sample obtained from the copolymerization of MMA/MAA (2/1, mol/mol) at 12 min of reaction (solid line) and at the end of reaction (dash dot line).

3.1.2. Molecular Weight. Figure 2 shows the molecular weight distribution (MWD) of the copolymer at early stage and at the end of polymerization. The corresponding values of number-average molecular weight (M_n) and weight-average molecular weight (M_w) along those of ES-100 are shown in Table 1. The MWD curves in Figure 2 show a slight shift toward the region of high molecular weight by passing the polymerization from low to high conversion, which is reflected in the small increase in the values of M_n and M_w.

Table 1: Average molecular weights of the copolymer in CNP and those of the commercial copolymer.

Sample	$M_n \times 10^{-5}$ (g/mol)	$M_w \times 10^{-5}$ (g/mol)
From copolymerization at 10.1% in conversion	2.17	4.92
At the end of copolymerization (88.2% in conversion)	2.31	5.11
ES-100	0.24	0.40

Such an increase was expected, taken into account the inverse relationship between the elution time of copolymer samples analyzed by GPC and conversion [14]. As already explained, the increase in molecular weight was ascribed to an extension of the growth interval of the copolymer chain, which would result from a slowdown in the bimolecular termination rate between the chain and the entry radical into the particles. This condition comes from a diminution in the radical entry rate, which is ascribed to a decrease in the ratio of radicals to particles in the aqueous medium.

On the other hand, in accordance with Table 1, it is evident that the copolymer prepared in this study has a greater molecular weight than that of commercial ES-100, which probably would lead to a longer dissolution time of CNP in the bloodstream.

Another important result is about the average number of chains per particle (N_c) at the end of the polymerization. This value, close to 1, was estimated by obtaining the number of moles in the particle (dividing the weight of one particle by M_n) and then multiplying by Avogadro's number (Av) using the following equation:

$$N_c = \frac{\pi \rho_{cp} D_n^3}{6 M_n} \mathrm{Av}, \tag{3}$$

where D_n is the number-average diameter at the end of the polymerization and ρ_{cp} is the density of the copolymer, estimated as 1.23 g/mL from the density values of 1.19 g/mL for poly(methyl methacrylate) [26] and 1.29 g/mL for poly(-methacrylic acid) [27].

3.1.3. Chemical Characterization. FTIR spectra of prepared CNP and the commercial ES-100 are simultaneously shown in Figure 3. It was observed that both samples have exactly the same characteristic bands, in accordance with that reported in the literature [28, 29]. The first signals between 2900 and 2800 cm^{-1} correspond to asymmetric and symmetrical stretching of C–H from CH_3 and CH_2 groups in the copolymer. At approximately 1720 cm^{-1}, both compounds share the same signal with a very similar high intensity that corresponds to the stretching vibration of C=O, typical in both carboxylic acid and ester groups. The CH_3 and CH_2 deformation vibrations can be observed in the region between 1490 and 1390 cm^{-1}. Finally, an intense signal corresponding to the C–O stretching of esters and carboxylic acids can be clearly identified at approximately 1150 cm^{-1} in both spectra. A partial conclusion of this analysis is that the copolymer that conforms the nanoparticles has a chemical composition qualitatively similar to that of the ES-100.

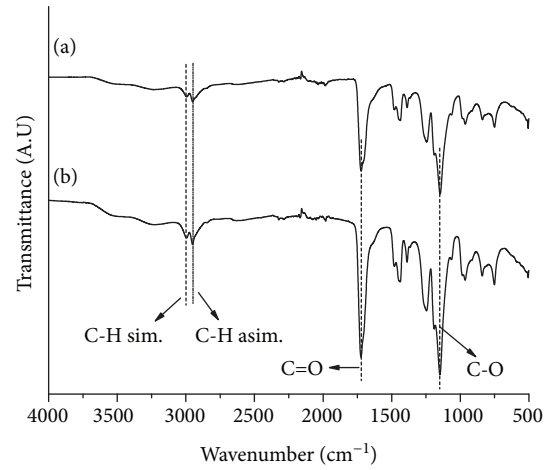

Figure 3: Infrared spectra of (a) a sample obtained from the copolymerization of MMA/MAA (2/1, mol/mol); (b) Eudragit S100.

To complement the chemical characterization of the CNP, a ^{13}C-NMR analysis was carried out to both CNP and ES-100; the corresponding carbonyl region of both spectra is shown in Figure 4. From these spectra, the MMA/MAA molar ratios for both copolymers were calculated using the integration of the signals corresponding to the carbonyl groups, which are approximately located at 180 ppm for the MMA and at 184 for the MAA. The MMA/MAA molar ratios thus obtained were 2.1 and 1.75 for ES-100 and CNP, respectively, which indicate that the copolymer in CNP has a slightly higher content of MAA units than those contained in ES-100. This fact suggests that the chains in CNP would be more quickly hydrolyzed and solubilized than those in ES-100 in organic fluids with pH higher than 7. However, the higher molecular weight of the copolymer (see Table 1) could counteract this expected behavior. Moreover, the higher content of MAA units ensures the hydrolysis of MMA units in the copolymer and, as consequence, the metabolization of the CNP by the organism in the manner similar to that reported for ES-100, that is, without causing harm to the body.

3.1.4. Stability. The latex resulting from the polymerization was dialyzed to remove residual monomers and surfactants. After dialysis, zeta potential of the CNP in the dispersion was determined at different pH. The results shown in Figure 5 depict an increase in zeta potential as pH increases, going from -21.4 to -50.0 mV when the pH increased from 3.8 to 7.5. This behavior is very interesting taking into account that even though the nanoparticles were left without the protection of the surfactant, they were very stable, as indicated by the high zeta potential. This stability probably arises

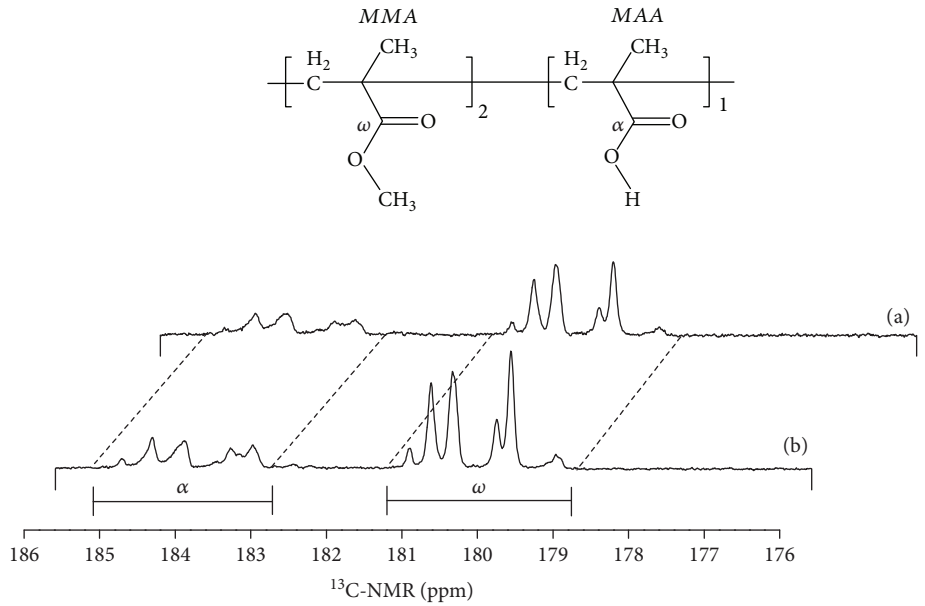

Figure 4: ^{13}C-NMR spectra of samples from copolymer MMA/MAA: (a) synthetized by semicontinuous heterophase polymerization; (b) Eudragit S100.

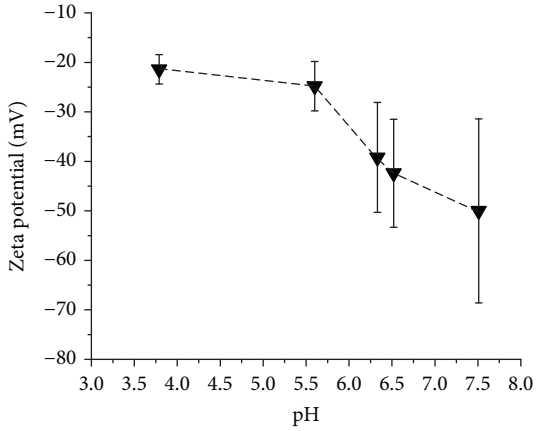

Figure 5: Zeta potential behavior of CNP from copolymerization of MMA/MAA (2/1, mol/mol) at different pH values.

from the carboxyl and ester groups provided by MAA and MMA units in the copolymer chains. It is well-known that polar groups like carboxyl and esters are able to protect polymer particles against coalescence [30]. In accordance with this, the direct relationship between zeta potential and pH could be assigned to an increase in the ionization, as pH increases, of the carboxyl groups in the copolymer chains oriented toward the particle surface to generate -COO- groups, which would lead to an augment in the negative charge on this surface.

3.2. ASA Loading in CNP

3.2.1. Loading. Figure 6 displays the results of loading CNP with ASA; Figure 6(a) indicates that ASA content in the CNP increases as the ASA content increments in the DCM solution, to reach around 20-22% when 0.4% drug content in the solution was used. On the other hand, the loading efficiency, in Figure 6(b), attains a maximum value of 36.5% at 0.2% ASA concentration in the DCM solution. This behavior could be explained as follows.

When the concentration of ASA in DCM goes from 0.1 to 0.2%, there is an increase in both the amount of ASA loaded in the nanoparticles as well as in the loading efficiency; this can be attributed to the fact that increasing the concentration of ASA in DCM increases the difference in chemical potential of ASA between the DCM solution and the vicinity of the CNP, which, according to Fick's law, favors the diffusion of ASA toward the CNP. In turn, this leads to a greater adsorption of ASA in CNP.

When the concentration of ASA in DCM solution is now increased to 0.4%, there is still an increase in the amount of ASA loaded in CNP; however, the decrease in efficiency is evident, and by further increasing the concentration of ASA in DCM solution, to 0.6%, the efficiency decreases even more. This behavior indicates that up to approximately 0.2% of ASA in the DCM solution, diffusion is the dominant mechanism in the loading process, while at higher concentrations, the adsorption rate of ASA in CNP becomes the controlling step, so that any subsequent increase in the diffusion, provoked by increasing the concentration of ASA in DCM solution, does not increase the loading on CNP. In fact, it would seem that at the loading conditions used in this study, 20-22% of ASA in loaded nanoparticles is the maximum load; this could be due to the fact that when this load is reached, there are no longer any functional groups from the copolymer available to form hydrogen bonds with the ASA molecules.

Under these circumstances, hydrogen bonds could only be established between the ASA molecules adsorbed on the surface of the nanoparticles and those located in their vicinity to increase the drug content; however, at the pH of 5, at

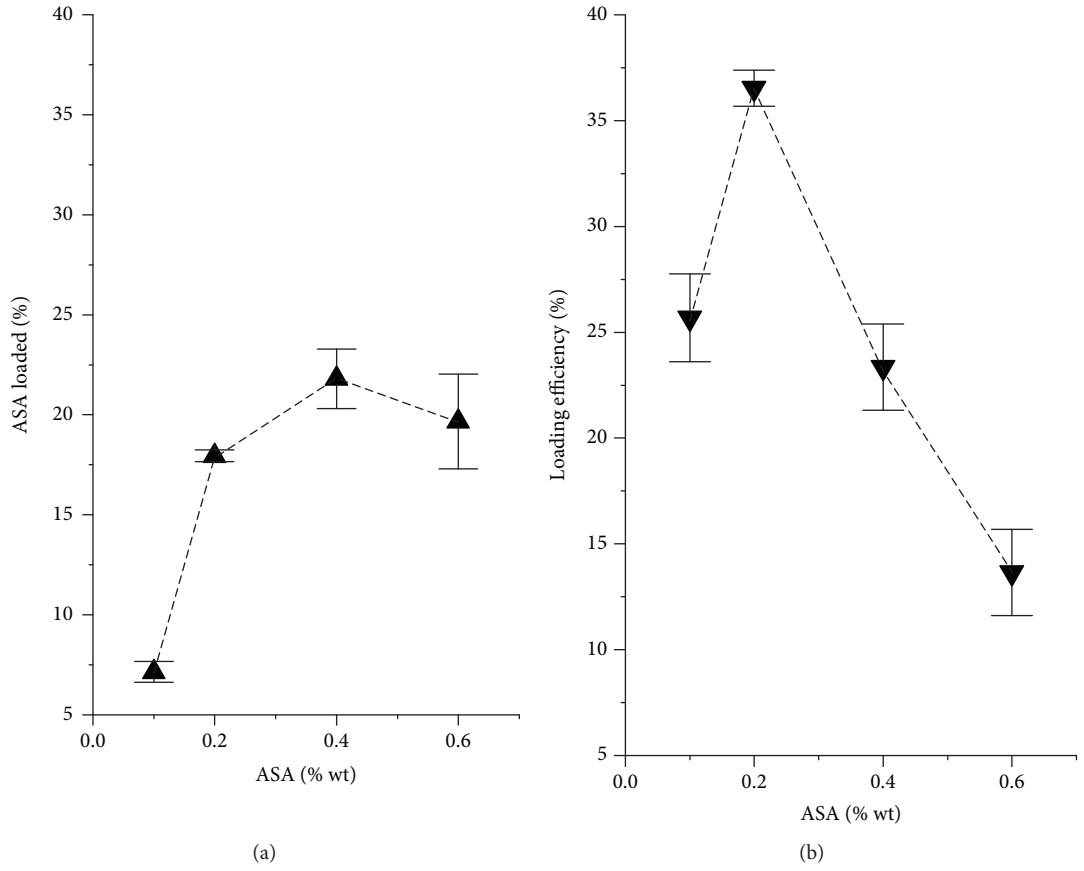

Figure 6: (a) ASA loaded in CNP and (b) ASA loading efficiency, as a function of drug concentration in the DCM solution.

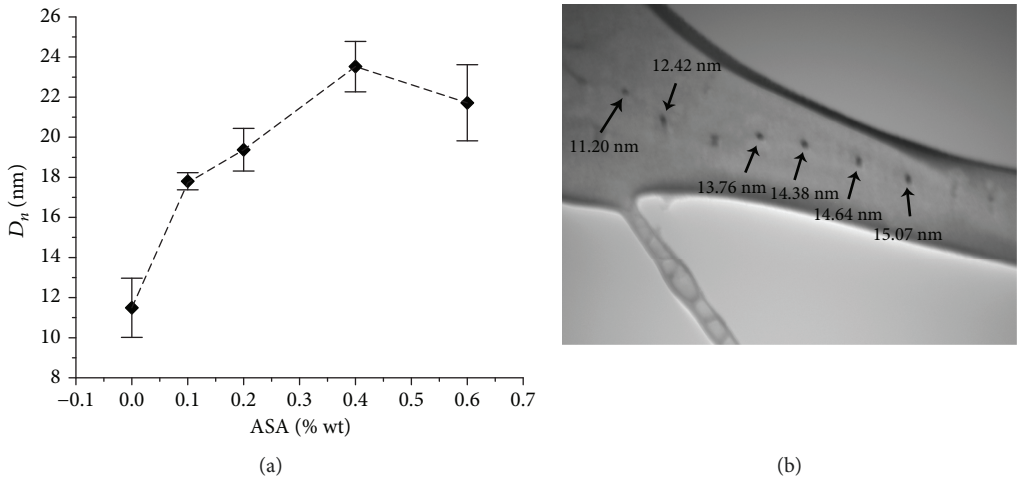

Figure 7: (a) D_n values of loaded nanoparticles, determined by QLS, of samples from the ASA loading at different drug concentration in the DCM solution; (b) TEM micrograph of loaded nanoparticles when 0.4% of ASA concentration in DCM was used.

which the loading was carried out, a great part of the carboxyl groups in the molecules of ASA ($pKa = 3.5$) [31], on the nanoparticle surface would be ionized and, therefore, negatively charged, which would cause repulsion between the ASA molecules, making it difficult to establish the hydrogen bonds between them and, adversely, affecting the loading of the drug. It is believed that this repulsion effect was lower during the adsorption of ASA on the CNP because the pKa of the carboxyl in MAA units is 6 [32]. This value is higher than that of ASA; therefore, the fraction of carboxyl groups on the CNP surface ionized at pH 5 would be less.

Starting from what has just been discussed, a strategy to increase the efficiency of ASA loading in nanoparticles would require carrying out, in a further research, the loading

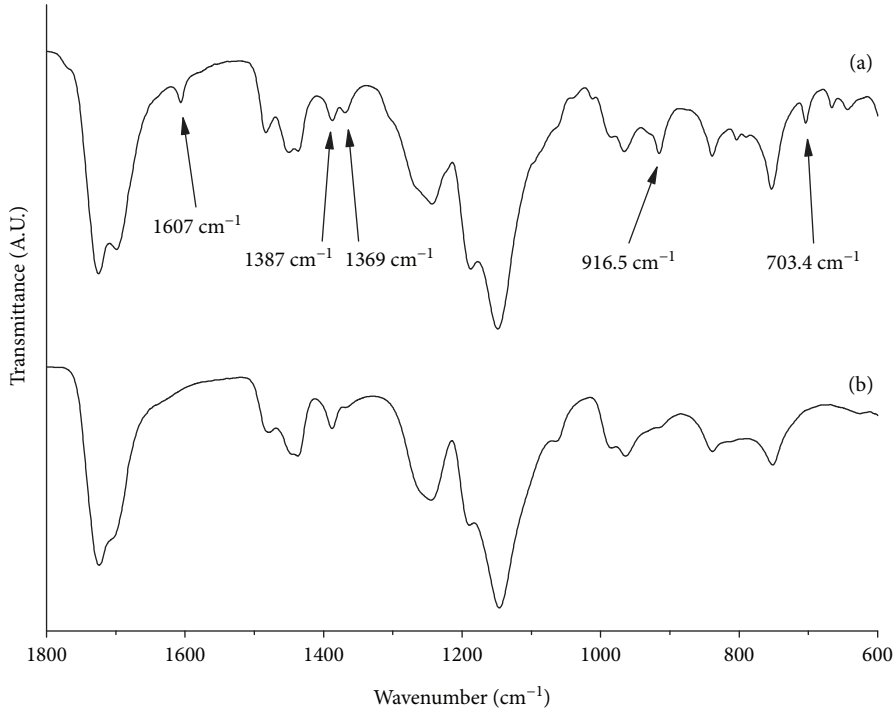

Figure 8: Infrared spectra of (a) ASA-loaded nanoparticles and (b) nanoparticles without load.

process at $pH < 5$ in order to induce a lower ionization degree of carboxyl groups on the CNP surface and, as consequence, having more H available to form H bonds. Once the surface of the CNP has been completely covered, a further decreasing of pH would decrease the ionization degree of carboxyl groups of ASA, leaving more H available to form hydrogen bonds between the molecules of ASA on the CNP surface and those arriving to the vicinity of the nanoparticles. The loading technique used in this study could be applied to the loading of other drugs in nanoparticles, besides ours, with carboxyl groups on their surface.

3.2.2. Particle Size. Figure 7 shows the sizes of ASA-loaded CNP obtained at different concentrations of drug in the DCM solutions. Figure 7(a) displays the QLS measurements, while Figure 7(b) shows a micrograph of the loaded nanoparticles obtained when the solution containing 0.4% of ASA was used. According to Figure 7(a), D_n increases as the drug content is higher, stabilizing around 22-23 nm, which contrasts with the sizes in Figure 7(b) where the nanoparticles with 21.8% of ASA show diameters between 11 and 15 nm. Starting from 12 nm in diameter for CNP, a simple calculation gives an estimated value of 13 nm for the expected size of the ASA-loaded nanoparticles with 21.8% in drug content. This value is roughly that observed in the micrograph in Figure 7(b). The reason for the difference between the results obtained by these techniques would probably come from a decrease in the nanoparticle stability as a result of the coating of their surface with ASA molecules causing some degree of nanoparticle flocculation; this would be reflected in an apparent increase in the size of ASA-loaded nanoparticles, which was determined within the next hour once the drug load is finished. This possible explanation arises from the fact that after 24 hours, the nanoparticle size measured by QLS reaches more than 100 nm in D_n, contrasting with the great stability of dialyzed CNP, which retain the size in aqueous dispersions for several months. This decrease in the stability of the ASA-loaded nanoparticles suggests that they must be dried soon after obtaining in order to conserve them before use.

The sizes obtained in this study for ASA-loaded nanoparticles are significantly lower than those reported in the literature, where ASA-loaded particles with diameters of tens [18, 23] and even hundreds of nanometers [17, 19–22, 24, 25] are common.

3.2.3. Chemical Characterization. The presence of ASA in the loaded nanoparticles was confirmed by FTIR, in accordance with Figure 8, which includes both the spectrum of loaded nanoparticles from the loading test with 0.4% of drug in the DCM solution, Figure 8(a), and that of CNP without load, Figure 8(b). When comparing these spectra, it is observed that the sample of loaded nanoparticles presents new signals in the wavenumber range of 1,800 to 600 cm^{-1}. The signal at 1607 cm^{-1} can be attributed to C=C type stretching, which is present only in the aromatic ring of the ASA, since the structure of the copolymer does not show any type of the unsaturated group C=C, neither linear nor aromatic. Complementing, the signals at 1,387 and 1,389 cm^{-1} correspond to C–C stretching vibration characteristic of aromatic compounds. The last two signals indicated by arrows in the loaded nanoparticle spectrum at 916.5 and 703.4 cm^{-1} correspond, respectively, to stretches of O–H of the carboxylic

group attached to the benzene ring of the structure of the ASA and C–H in the benzene ring [18, 33, 34].

4. Conclusions

Nanoparticles with 12 nm in diameter of the poly(MMA-*co*-MAA) were prepared to be loaded with ASA. The chemical characterization shows that the MMA/MAA molar ratio is 1.75/1, that is, a little lower than that of ES-100. However, it is believed that this fact does not affect the biodegradability and metabolization without toxic effects of this copolymer, since its higher content of MAA would facilitate its hydrolysis and subsequent dissolution in the body's aqueous fluids with pH greater than 7. The preparation of nanoparticles loaded with 22% of ASA with an apparent diameter of 23.5 nm determined by QLS was achieved. However, the STEM results indicate that in reality, the loaded nanoparticles would have a diameter between 11 and 15 nm. The larger size obtained by QLS would probably come from a reversible aggregation of the nanoparticles caused by the decrease in their stability when covered by ASA.

Due to the so small size of the ASA-loaded nanoparticles obtained in this study, it is thought that they could be used as a basis for a new form of ASA administration. However, further research is required to achieve such a purpose.

Data Availability

The data used to support the findings of this study are included within the article.

Conflicts of Interest

The authors declare that there is no conflict of interest regarding the publication of this paper.

Acknowledgments

We are grateful to Daniel Alvarado and José Luis de la Peña for their technical assistance. The authors would like to express their acknowledgment to the Laboratorio Nacional de Materiales Grafénicos (232753) from CONACYT for its support in characterization of samples. CONACYT supported this research through grant CB-2013-223227.

References

[1] R. Sunasee, C. K. Adokoh, J. Darkwa, and R. Narain, "Therapeutic potential of carbohydrate-based polymeric and nanoparticle systems," *Expert Opinion on Drug Delivery*, vol. 11, no. 6, pp. 867–884, 2014.

[2] C. I. C. Crucho, "Stimuli-responsive polymeric nanoparticles for nanomedicine," *ChemMedChem*, vol. 10, no. 1, pp. 24–38, 2015.

[3] J. Ahlawat, G. Henriquez, and M. Narayan, "Enhancing the delivery of chemotherapeutics: role of biodegradable polymeric nanoparticles," *Molecules*, vol. 23, no. 9, article 2157, 2018.

[4] H. Choudhury, B. Gorain, M. Pandey, R. K. Khurana, and P. Kesharwani, "Strategizing biodegradable polymeric nanoparticles to cross the biological barriers for cancer targeting," *International Journal of Pharmaceutics*, vol. 565, pp. 509–522, 2019.

[5] J. Wang, X. Hu, and D. Xiang, "Nanoparticle drug delivery systems: an excellent carrier for tumor peptide vaccines," *Drug Delivery*, vol. 25, no. 1, pp. 1319–1327, 2018.

[6] J. B. Vines, D.-J. Lim, and H. Park, "Contemporary polymer-based nanoparticle systems for photothermal therapy," *Polymers*, vol. 10, no. 12, article 1357, 2018.

[7] P. Martins, D. Rosa, A. R. Fernandes, and P. V. Baptista, "Nanoparticle drug delivery systems: recent patents and applications in nanomedicine," *Recent Patents on Nanomedicine*, vol. 3, no. 2, pp. 105–118, 2014.

[8] S. Akhter, I. Ahmad, M. Z. Ahmad et al., "Nanomedicines as cancer therapeutics: current status," *Current Cancer Drug Targets*, vol. 13, no. 4, pp. 362–378, 2013.

[9] V. P. Torchilin, "Multifunctional, stimuli-sensitive nanoparticulate systems for drug delivery," *Nature Reviews Drug Discovery*, vol. 13, no. 11, pp. 813–827, 2014.

[10] D. Rosenblum, N. Joshi, W. Tao, J. M. Karp, and D. Peer, "Progress and challenges towards targeted delivery of cancer therapeutics," *Nature Communications*, vol. 9, no. 1, pp. 1–12, 2018.

[11] M. E. Davis, "Fighting cancer with nanoparticle medicines-the nanoscale matters," *MRS Bulletin*, vol. 37, no. 9, pp. 828–835, 2012.

[12] T. Kissel and M. Roser, "Influence of chemical surface-modification on the phagocytic properties of albumin nanoparticles," *Proceedings International Symposium Controlled Release Bioactive Materials*, vol. 18, pp. 275-276, 1991.

[13] P. Tartaj, M. P. Morales, S. Veintemillas-Verdaguer, T. Gonz lez-Carre o, and C. J. Serna, "The preparation of magnetic nanoparticles for applications in biomedicine," *Journal of Physics D: Applied Physics*, vol. 36, no. 13, pp. R182–R197, 2003.

[14] H. Saade, M. L. Guillén, J. C. Romero et al., "Biocompatible and biodegradable ultrafine nanoparticles of poly(methyl methacrylate-*co*-methacrylic acid) prepared via semicontinuous heterophase polymerization: kinetics and product characterization," *International Journal of Polymer Science*, vol. 2016, Article ID 7674620, 8 pages, 2016.

[15] A. Sonje and A. Chandra, "Comprehensive review on Eudragit polymers," *International Research Journal of Pharmacy*, vol. 4, no. 5, pp. 71–74, 2013.

[16] H. Saade, R. Diaz de León-Gómez, F. J. Enríquez-Medrano, and R. G. López, "Preparation of ultrafine poly(methyl methacrylate-*co*-methacrylic acid) biodegradable nanoparticles loaded with ibuprofen," *Journal of Biomaterials Science, Polymer Edition*, vol. 27, no. 11, pp. 1126–1138, 2016.

[17] M. González, J. Rieumont, D. Dupeyron et al., "Nanoencapsulation of acetyl salicylic acid within enteric polymer nanoparticles," *Reviews on Advanced Materials Science*, vol. 17, pp. 71–75, 2008.

[18] S. Jin, L. Feng, and X. Yu, "Preparation and characterization of aspirin/chitosan nanoparticles by nucleation and ionic cross-linking in micro emulsions," *Journal of Controlled Release*, vol. 152, pp. e39–e41, 2011.

[19] S. Das, J. R. Bellare, and R. Banerjee, "Protein based nanoparticles as platforms for aspirin delivery for ophthalmologic applications," *Colloids and Surfaces B: Biointerfaces*, vol. 93, pp. 161–168, 2012.

[20] A. Saritha Reddy and A. Krishna Sailaja, "Preparation and characterisation of aspirin loaded ethylcellulose nanoparticles by solvent evaporation technique," *World Journal of Pharmaceutical Sciences*, vol. 3, pp. 1781–1793, 2014.

[21] L. Zhou, X. Duan, S. Zeng et al., "Codelivery of SH-aspirin and curcumin by mPEG-PLGA nanoparticles enhanced antitumor activity by inducing mitochondrial apoptosis," *International Journal of Nanomedicine*, vol. 10, pp. 5205–5218, 2015.

[22] A. Krishna Sailaja, "In vitro dissolution studies of aspirin loaded gelatine nanoparticles by desolvation technique using acetone as desolvating agent," *CIBTech Journal of Pharmaceutical Sciences*, vol. 4, pp. 1–13, 2015.

[23] S. Luo, H. Man, X. Jia et al., "Preparation and characterization of acetylsalicylic acid/chitosan nanoparticles and its antithrombotic effects," *Designed Monomers and Polymers*, vol. 21, no. 1, pp. 172–181, 2018.

[24] S. Akkad and C. J. Serpell, "Degradable polymers and nanoparticles built from salicylic acid," *Macromolecular Rapid Communications*, vol. 39, no. 14, article 1800182, 2018.

[25] L. Lei, Z. Liu, P. Yuan et al., "Injectable colloidal hydrogel with mesoporous silica nanoparticles for sustained co-release of microRNA-222 and aspirin to achieve innervated bone regeneration in rat mandibular defects," *Journal of Materials Chemistry B*, vol. 7, no. 16, pp. 2722–2735, 2019.

[26] W. Wunderlich, "Physical constants of poly(methyl methacrylate)," in *Polymer Handbook*, J. Brandrup, E. H. Immergut, and E. A. Grulke, Eds., pp. V/87–V/90, John Wiley & Sons, New York, NY, USA, 4th edition, 2003.

[27] J. Wen, "Poly(methacrylic acid)," in *Polymer Data Handbook*, J. E. Mark, Ed., pp. 638–640, Oxford University Press, New York, NY, USA, 1st edition, 1999.

[28] C. R. E. Mansur and E. E. C. Monteiro, "Characterization of methacrylic polymers by calorimetry and infrared analyses," *Journal of Applied Polymer Science*, vol. 68, no. 3, pp. 345–354, 1998.

[29] E. S. Rufino and E. E. C. Monteiro, "Infrared study on methyl methacrylate-methacrylic acid copolymers and their sodium salts," *Polymer*, vol. 44, no. 23, pp. 7189–7198, 2003.

[30] M. J. Ballard, R. G. Gilbert, D. H. Napper, P. J. Pomery, P. W. O'Sullivan, and J. H. O'Donnell, "Propagation rate coefficients from electron spin resonance studies of the emulsion polymerization of methyl methacrylate," *Macromolecules*, vol. 19, no. 5, pp. 1303–1308, 1986.

[31] K. Kanani, S. C. Gatoulis, and M. Voelker, "Influence of differing analgesic formulations of aspirin on pharmacokinetic parameters," *Pharmaceutics*, vol. 7, no. 3, pp. 188–198, 2015.

[32] W. Guo and N. Hu, "Interaction of myoglobin with poly(-methacrylic acid) at different pH in their layer-by-layer assembly films: an electrochemical study," *Biophysical Chemistry*, vol. 129, no. 2-3, pp. 163–171, 2007.

[33] B. H. Stuart, "Infrared Spectroscopy: Fundamentals and Applications," in *Analytical Techniques in the Sciences*, Wiley, New York, NY, USA, 1st edition, 2004.

[34] K. Mphahlele, M. S. Onyango, and S. D. Mhlanga, "Adsorption of aspirin and paracetamol from aqueous solution using Fe/N-CNT/β-cyclodextrin nanocomopsites synthesized via a benign microwave assisted method," *Journal of Environmental Chemical Engineering*, vol. 3, no. 4, pp. 2619–2630, 2015.